Sigma-electrons responsible for cooperativity and ring equalization in hydrogen-bonded supramolecular polymers

Santos, L.D.; Cesario, D.; Vermeeren, P.; Lubbe, S.C.C. van der; Nunzi, F.; Fonseca Guerra, C.

σ-Electrons Responsible for Cooperativity and Ring Equalization in Hydrogen-Bonded Supramolecular Polymers

Lucas de Azevedo Santos[+],[a] Diego Cesario[+],[a, b] Pascal Vermeeren,[a] Stephanie C. C. van der Lubbe,[a] Francesca Nunzi,[b, c] and Célia Fonseca Guerra*[a, d]

We have quantum chemically analyzed the cooperative effects and structural deformations of hydrogen-bonded urea, deltamide, and squaramide linear chains using dispersion-corrected density functional theory at BLYP-D3(BJ)/TZ2P level of theory. Our purpose is twofold: (i) reveal the bonding mechanism of the studied systems that lead to their self-assembly in linear chains; and (ii) rationalize the C–C bond equalization in the ring moieties of deltamide and squaramide upon polymerization. Our energy decomposition and Kohn-Sham molecular orbital analyses reveal cooperativity in all studied systems, stemming from the charge separation within the σ-electronic system by charge transfer from the carbonyl oxygen lone pair donor orbital of one monomer towards the σ* N–H antibonding acceptor orbital of the neighboring monomer. This key orbital interaction causes the C=O bonds to elongate, which, in turn, results in the contraction of the adjacent C–C single bonds that, ultimately, makes the ring moieties of deltamide and squaramide to become more regular. Notably, the π-electron delocalization plays a much smaller role in the total interaction between the monomers in the chain.

Introduction

In recent years, molecular self-assembly has received much attention due to its importance in biological systems, supramolecular chemistry, and the rational design and synthesis of materials.[1] The term self-assembly defines a spontaneous process causing the association of molecules via intermolecular interactions.[2] Recent studies have demonstrated cooperativity in the self-assembly of hydrogen-bonded nucleobases and linear chains.[3] That is, the hydrogen-bond strength of these systems containing *n* monomers is substantially higher than (*n*−1) times the hydrogen-bond strength of the corresponding dimer. The origin of this cooperative effect can be traced back to the nature of the hydrogen bonds. Besides the attractive electrostatic interaction between oppositely charged atoms, donor–acceptor interactions between the lone pair of a nitrogen or oxygen atom and the accepting σ* orbital on the N–H group also contribute to the strength of hydrogen bonds.[4] In the case of linear hydrogen-bonded chains, with all hydrogen bonds pointing in the same direction, this leads to a net charge accumulation on the terminal monomers of the chain, resulting in more stabilizing electrostatic interactions and a reduction of the HOMO–LUMO gap between the σ-orbitals upon increasing the chain length and, ultimately, in more stabilizing orbital interactions.[3]

Next to the prior described explanation for the origin of cooperativity, another viewpoint has been proposed based on the resonance-assisted hydrogen bonds (RAHB) model.[5] This model attributes the source of cooperativity upon polymerization to the π-electron delocalization, since the hydrogen-bond strength has a good correlation with the increase in π-delocalization energy across the system.[5b] Furthermore, geometrical deformations upon self-assembly have been also attributed to the presence of π-conjugation. For example, squaramide, which is an important molecular entity for drug discovery and molecular recognition, forms linear polymers via a double hydrogen bond between the two NH_2 hydrogen-bond donor groups and the two C=O hydrogen-bond acceptor groups (see Scheme 1).[6] Interestingly, the C–C bond lengths in the four-membered ring of a squaramide monomer become more equal when the number of monomers in the chain increases,[7] and this structural reorganization is thought to be related to the gain in aromaticity as a response to the

[a] L. de Azevedo Santos,[+] Dr. D. Cesario,[+] P. Vermeeren, Dr. S. C. C. van der Lubbe, Prof. Dr. C. Fonseca Guerra
Department of Theoretical Chemistry, Amsterdam Institute for Molecular and Life Sciences (AIMMS)
Amsterdam Center for Multiscale Modeling (ACMM)
Vrije Universiteit Amsterdam
De Boelelaan 1083, 1081 HV Amsterdam (The Netherlands)
E-mail: c.fonsecaguerra@vu.nl
[b] Dr. D. Cesario,[+] Dr. F. Nunzi
Department of Chemistry, Biology and Biotechnology
University of Perugia, Via Elce di Sotto 8, I-06123 Perugia (Italy)
[c] Dr. F. Nunzi
Istituto di Scienze e Tecnologie Chimiche "Giulio Natta" (CNR-SCITEC), Via Elce di Sotto 8, 06123, Perugia (Italy)
[d] Prof. Dr. C. Fonseca Guerra
Leiden Institute of Chemistry, Gorlaeus Laboratories
Leiden University
Einsteinweg 55, 2333 CC Leiden (The Netherlands)
[+] These authors contributed equally to this work.

Supporting information for this article is available on the WWW under https://doi.org/10.1002/cplu.202100436

This article is part of a Special Collection celebrating the 10th Anniversary of ChemPlusChem.

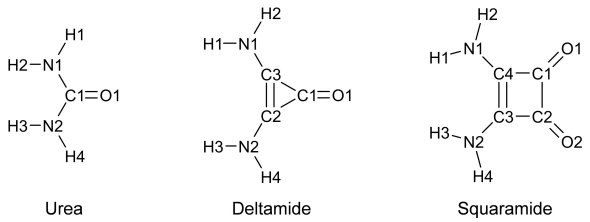

Scheme 1. Schematic structures for the urea, deltamide, and squaramide monomers.

enhancement of π-electron delocalization.[8] Previous studies of Shaik[9a] and Bickelhaupt,[9b] however, revealed that this assumed causal relationship between aromaticity and π-electronic system is incorrect. They have both, independently, shown that the aromatic ring equalization of the molecule benzene stems from the σ-electronic system and not the π-electronic system, *i.e.*, π-electron delocalization, as described above.

The present theoretical work will focus on the bonding mechanism of hydrogen-bonded linear chains based on three different monomers (see Scheme 1). To this end, we have studied the linear chain formation of urea, deltamide, and squaramide using quantitative Kohn-Sham molecular orbital (KS-MO) theory combined with a matching canonical energy decomposition analysis (EDA) scheme.[10] We find that all investigated linear chains exhibit cooperativity, which is caused by the charge transfer within the σ-system, and not the π-system as originally proposed using RAHB.[5] In addition, our analysis elucidates the structural reorganization of the ring motifs of deltamide and squaramide upon polymerization and reveals that the equalization of the C–C bonds is originating from the elongation of the C=O bonds induced by the hydrogen bonding with the neighboring monomer.

Results and Discussion

Polymeric structure and hydrogen-bond strength

The calculated equilibrium geometries of the isolated urea, deltamide, and squaramide with C_S symmetry, as well as the geometries they acquire in an infinite linear chain are shown in Figure 1. The fully optimized monomers at C_1 symmetry (*i.e.*, without any symmetry constraints) deviate only slightly, up to 0.6 kcal mol^{-1}, from their respective C_S structures with the mirror plane through all atoms of the molecule (see Table S1). The isolated urea, deltamide, and squaramide are not perfectly planar due to the pyramidalization of the NH_2 groups. The fully optimized dimers with C_1 symmetry yield the same energy as the dimers with C_S symmetry (see Table S1). So, employing planarity to these systems allows us to mimic well-known supramolecular polymers[8a]. Since the use of C_S symmetry allows us to separate the σ- and π-orbital interactions, all linear chains were enforced to be planar (C_S symmetry) in our computations.

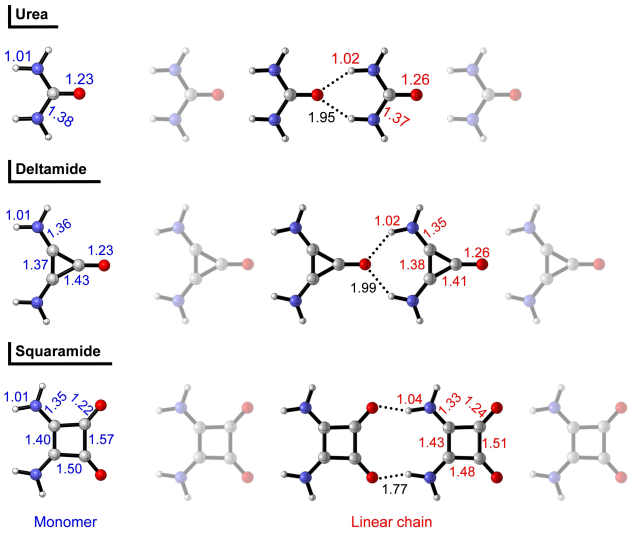

Figure 1. Geometries and bond lengths (in Å) of urea, deltamide, and squaramide in the optimized monomer (left) and in an infinite long linear chain (right) with C_S symmetry.

The geometries of the infinite long linear chains were obtained using BAND module at BLYP-D3(BJ)/TZ2P level under C_S symmetry (see computational details in the Theoretical Methods). Each monomer binds via a C=O···H–N hydrogen bond to the adjacent monomers and acts as both a hydrogen bond donor as well as acceptor. The urea and deltamide linear chains have one hydrogen bond acceptor, namely, one carbonyl oxygen, on each monomer and engage into a bifurcated hydrogen bond with the two amine groups of the adjacent monomer. The corresponding hydrogen bond lengths, defined as the distance between the carbonyl oxygen and the hydrogen atom of the amine, are for both the urea and deltamide linear chains close to 2 Å (see Table 1). In the squaramide linear chain, on the other hand, the monomers consist of two carbonyl oxygens, which both undergo hydrogen bonding with the amine of the neighboring monomer, leading to a significantly shorter hydrogen bond of 1.77 Å.

Upon the formation of the linear chains, we observe two important structural reorganizations in the monomers. First, for all infinite linear chains, the C=O and N–H bonds, that participate in the hydrogen bonds, become longer.[11] For instance, for the urea linear chain, the C=O bond elongates from 1.23 Å in the optimized monomer to 1.26 Å in the linear

Table 1. Hydrogen bond distances (in Å), total interaction energies (in kcal mol^{-1}) for the dimer and decamer, the average bond strength in the decamer (in kcal mol^{-1}), and the average synergy in the decamer (in kcal mol^{-1}).[a,b]

Linear chain	$r_{O\cdots H}$	ΔE_{int}^{dimer}	$\Delta E_{int}^{decamer}$	$\Delta E_{int}^{decamer}/9$	$\Delta E_{syn}^{decamer}$
Urea	1.95	−10.0	−127.0	−14.1	−4.1
Deltamide	1.99	−13.6	−164.8	−18.3	−4.7
Squaramide	1.77	−16.3	−215.6	−24.0	−7.7

[a] Computed at BLYP-D3(BJ)/TZ2P. [b] Total interaction energies of the linear chain ranging from the dimer to the decamer can be found in Table S2.

chain, and the N–H bond slightly stretches from 1.01 Å in the optimized monomer to 1.02 Å in the linear chain. Second, the formation of the linear deltamide and squaramide chains result in an equalization of the C–C bond lengths in the three- and four-membered rings, respectively (see Figure 1). That is, the C=C double bonds of deltamide (C2=C3) and squaramide (C3=C4) elongate by 0.01 and 0.03 Å, respectively (see Scheme 1), while all C–C single bonds become shorter with a maximum shortening of 0.06 Å for the C1–C2 bond in squaramide. This, ultimately, leads to a more regular ring motif in each monomer of the linear chain. We also note a slight contraction for the N–C bonds, that shortens by 0.01, 0.01, and 0.02 Å for the urea, deltamide, and squaramide, respectively.

To identify a cooperative effect in the hydrogen bonds, the interaction energy was calculated for chains with varying sizes. The total interaction energies ΔE_{int} of the dimer and decamer linear chains for urea, deltamide, and squaramide, taken from their respective infinite chains, are shown in Table 1. The ΔE_{int} becomes increasingly more stabilizing, for both the dimer and decamer, when going from urea to deltamide to squaramide linear chains. Interestingly, this does not follow the trend of the hydrogen bond lengths in the different chains (see Figure 1), since the chain build-up from deltamide monomers does not have the weakest interaction energy, although it has the longest hydrogen-bond length. This shows that longer hydrogen bonds do not always imply weaker bonds.

The average interaction energy in the decamer, *i.e.*, $\Delta E_{int}^{decamer}$ divided by its 9 connections, is significantly more stabilizing than the interaction energy in the dimer, ΔE_{int}^{dimer}. This extra gain in stabilization is measured by the average synergy, ΔE_{syn} [see Eq. (4)], which is −4.1, −4.7, and −7.7 kcal mol^{-1}, respectively, for the urea, deltamide, and squaramide decamers (Table 1). The significant stabilizing effect on the hydrogen bonding between the monomers when the chain length increases from the dimer to the decamer is the direct proof that all systems studied in this work exhibit cooperativity. Figure 2 illustrates graphically the increase in stabilization, *i.e.*, the average synergy ΔE_{syn}, upon systematically increasing the chain length from the dimer to the decamer. The ΔE_{syn} curves of the urea and deltamide chains descend less steep than that of the squaramide chain, revealing that the former two systems exhibit less cooperativity than the latter. Notably, all ΔE_{syn} curves flatten upon increasing the chain size and the average synergy approaches its asymptotic value around ten monomers, that is, the decamer.

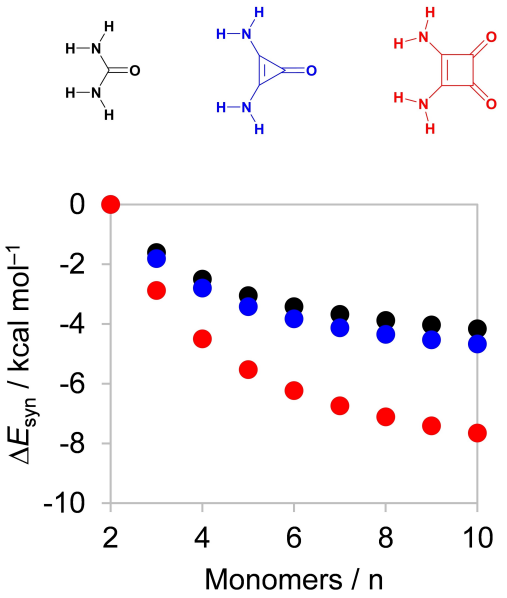

Figure 2. Average synergy of the interaction energy (in kcal mol^{-1}) for urea (black), deltamide (blue), and squaramide (red) linear chains, where every monomer is a separate fragment. Computed at BLYP-D3(BJ)/TZ2P.

Nature of bonding in dimers

To fully understand the bonding mechanism underlying the cooperative self-assembly of the hydrogen bonds in the studied linear chains, we first analyze the formation of the urea, deltamide, and squaramide dimers ($n=2$), where the geometries are taken from their respective infinite linear chains (Figure 3; see Table S3 and Figure S1 for the analyses on the fully optimized dimers at C_S symmetry). To this end, we have performed the energy decomposition analysis (EDA)[10] which decomposes the interaction energy ΔE_{int} into four different components: the usually attractive electrostatic interaction term ΔV_{elstat}, the steric Pauli repulsion ΔE_{Pauli}, the orbital interaction energy ΔE_{oi}, and the dispersion energy ΔE_{disp} (see Bond analysis in the Theoretical Methods for detailed description). The corresponding EDA results for the urea, deltamide, and squaramide dimers is graphically illustrated in Figure 3, in which we show the magnitude of each EDA term upon systematically elongating the hydrogen-bond distance $r_{O\bullet\bullet\bullet H}$ in equidistant steps by 0.6 Å, while keeping all other geometrical parameters frozen. Notably, the ΔE_{disp} is small (−2.4, −2.9, and −3.4 kcal mol^{-1} for urea, deltamide, and squaramide dimers, respectively) and varies less than 1.5 kcal mol^{-1} upon varying $r_{O\bullet\bullet\bullet H}$, and this term has, therefore, been omitted in this analysis.

Our analyses in Figure 3 reveal the significant covalent nature of the hydrogen bonds on top of stabilizing electrostatic attraction, as observed in previous work on hydrogen bonds.[12] For example, at the hydrogen-bond distance of the infinite linear chain, the total orbital interactions ΔE_{oi} for the urea, deltamide, and squaramide dimers are −7.8, −8.3, and −15.5 kcal mol^{-1}, respectively, whereas the corresponding electrostatic interactions ΔV_{elstat} are −16.6, −19.4, and −27.2 kcal mol^{-1}. Most importantly, we note that the orbital interactions stem, in line with our previous studies,[3,13] mainly from the σ-system, and not the π-system. In the geometry of the linear chain, the σ-orbital interactions represent around 30% of their total attractive component for the studied hydrogen-bonded dimers ($\Delta V_{elstat} + \Delta E_{oi}$). For example, the σ-contribution of the total orbital interactions, $\Delta E_{oi,\sigma}$, is −7.0, −7.3, and −13.6 kcal mol^{-1}, whereas the π-contribution, $\Delta E_{oi,\pi}$, which accounts for the π-delocalization, is only −0.8, −1.0, and −1.9 kcal mol^{-1} for the urea, deltamide, and squaramide dimer, respectively. The minor contribution of the π-electron delocali-

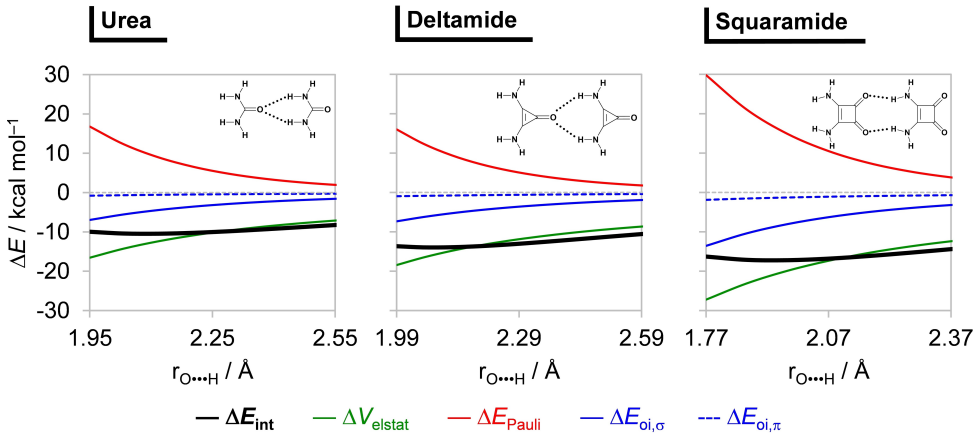

Figure 3. Energy decomposition analysis diagrams (in kcal mol^{-1}) for the urea, deltamide, and squaramide dimers at C_s symmetry, where geometries are taken from their respective infinite chains, projected onto the hydrogen-bond distance $r_{O\cdots H}$ (in Å), where all geometrical parameters of the monomers kept frozen, computed at BLYP-D3(BJ)/TZ2P. See Figure S1 for similar analyses on the geometrically relaxed dimers.

zation becomes even more pronounced when examining the energy decomposition terms upon varying the hydrogen-bond distance. Note that, for the studied hydrogen-bonded dimers, the $\Delta E_{oi,\sigma}$ curves descend much steeper than the $\Delta E_{oi,\pi}$ curves as $r_{O\bullet\bullet\bullet H}$ shortens. The correlation found in other studies between the strengthening of the hydrogen bonds and the gain in stabilization by the π-delocalization [5b] is also seen in Figure 3. However, our findings show that the π-electronic system is energetically less important than the σ-system, that is, the π-electrons do not significantly strengthen the hydrogen bond upon the formation of the dimer.

Figure 4 shows the KS-MO analyses for the donor–acceptor interactions within the σ-system for urea, deltamide, and squaramide dimers (see Figure S2 for the complete KS-MO diagram). The orbital interactions within the σ-system are mainly due to the charge transfer from the lone pair (LP) orbital of one monomer (σ_{HOMO-1} in urea and deltamide, σ_{HOMO-3} in squaramide) to the σ^*_{LUMO} of the second monomer, which has a significant N–H antibonding character. The squaramide dimer has an additional orbital interaction between the σ_{HOMO-2} and the σ^*_{LUMO+1} due to the presence of the two carbonyl groups (Figure 4c). Note that the σ_{HOMO-3} and σ_{HOMO-2} LP orbitals of the squaramide are not the energetically highest-lying LP orbitals (see Figure S2). However, σ_{HOMO-3} and σ_{HOMO-2} do have a larger donor–acceptor orbital overlap with the σ^*_{LUMO} and σ^*_{LUMO+1} unoccupied orbitals on the N–H groups compared to the energetically higher-lying σ_{HOMO-1} and σ_{HOMO} LPs (see Figure S2 for the values of overlap *S*). Herein, we can also understand the first important structural reorganization within the monomers. The σ_{HOMO-3} donor orbitals have a strong σ bonding character between the carbonyl C and O and lose ca. 0.01 electron upon hydrogen bonding. This loss of charge in a σ-type C=O bonding orbital slightly weakens and, thus, elongates the C=O bond. On the other hand, the N–H bond becomes longer due to the gain of charge (ca. 0.01 electron) in a σ*-type N–H antibonding orbital.

Cooperativity in the hydrogen-bonded linear chains

Next, we investigate the origin of cooperativity by performing an energy decomposition analysis (EDA) on the linear chains (Table 2) and calculating the average synergy corresponding to each interaction term, $\Delta V_{syn,elstat}$, $\Delta E_{syn,Pauli}$, $\Delta E_{syn,oi}$, and $\Delta E_{syn,disp}$ (see Figure 5, and Eq. (5) in the Theoretical Methods), upon formation of the chain from single monomers. For example, the $\Delta V_{syn,elstat}$ is obtained as the difference between the average electrostatic interaction ΔV_{elstat} of the *n*-monomer chain and the ΔV_{elstat} of the dimer, that is, $[\Delta V_{elstat}{}^{chain}/(n-1)]-\Delta V_{elstat}{}^{dimer}$.

The increasingly stabilizing average synergy ΔE_{syn} for the longer chains (*vide supra*) comes mainly from the orbital interactions within the σ-system, $\Delta E_{syn,oi,\sigma}$, that becomes more stabilizing when going from the dimer to the tetramer (see Figure 5). The average synergy of the orbital interactions within the π-system, $\Delta E_{syn,oi,\pi}$, has a minor contribution to cooperativity, whereas $\Delta E_{syn,Pauli}$ and $\Delta E_{syn,disp}$ are nearly zero and, therefore, have been omitted from the plots (see Table S4 in the Supporting Information). The average synergy of the electrostatic attraction $\Delta V_{syn,elstat}$ is also slightly more negative for the longer chains (see Figure 5). That is, the electrostatic attraction between *n* unperturbed monomers is already stronger than *n* times the electrostatic attraction between two monomers before any charge transfer occurs across the linear chain. The reason for this is that one monomer is not only affected by the electric field of the next adjacent monomer but also experiences long-range electrostatic interactions with non-neighboring monomers along the chain.

Next, we investigate a realistic experimental situation where the chain gradually grows from dimer to trimer to tetramer, by systematically adding a monomer to the hydrogen-bond acceptor side of the chain. We find that both ΔV_{elstat} and ΔE_{oi} become increasingly more stabilizing when the urea, deltamide, and squaramide linear chains lengthen (Table 2). Again, the gain in stabilization from the orbital interactions comes predominantly from the σ-system, $\Delta E_{oi,\sigma}$, whereas $\Delta E_{oi,\pi}$ only slightly strengthens when *n* goes from 2 to 4. For example,

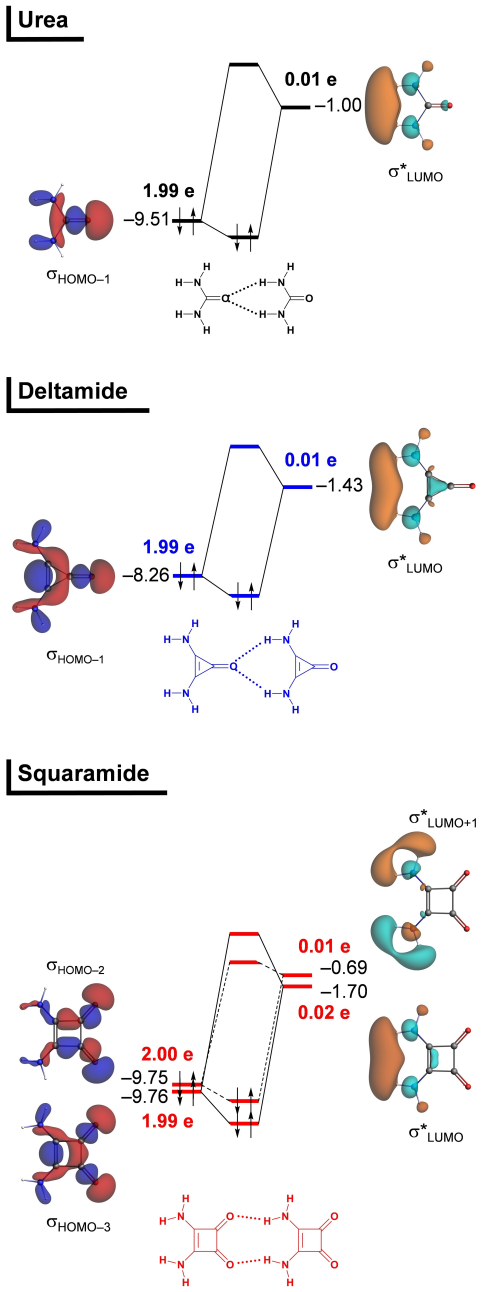

Figure 4. Molecular orbital diagram (energies in eV and gross Mulliken populations in electrons) of the formation of urea dimer, deltamide dimer, and squaramide dimer, computed at BLYP-D3(BJ)/TZ2P. Complementary fragment molecular orbitals shown in Figure S2 in the Supporting Information.

when *n* goes from 2 to 4 monomers for the squaramide linear chain, ΔV_{elstat} strengthens from −27.2 to −33.2 kcal mol^{-1}, $\Delta E_{oi,\sigma}$ becomes stronger from −13.6 to −15.3 kcal mol^{-1}, and $\Delta E_{oi,\pi}$ only strengthens from −1.9 to −2.3 kcal mol^{-1}. The charge transfer via donor–acceptor interactions causes two major effects in the studied linear chains. First, the accumulation of electronic density on one terminus of the chain leads to a destabilization of the LP orbitals on this monomer, while the depletion of electronic density on the other terminus leads to a stabilization of the σ^*_{LUMO} acceptor orbital on the pertinent monomer. For example, when the chain lengthens from the dimer to the tetramer, the σ_{HOMO-3} LP donor orbital in the squaramide chain goes from −9.8 to −8.3 eV, and the σ^*_{LUMO} acceptor orbital goes from −1.7 to −2.8 eV (see Table 2). Consequently, the orbital interactions between the chain and the next incoming monomer are enhanced due to a smaller energy gap between the donating and accepting orbitals, resulting in more stabilizing hydrogen bonds. The second effect resulting from the hydrogen bond interactions is the charge separation along the linear chain. As the charge flow from one end of the chain towards the other terminal monomer increases upon lengthening of the chain, the hydrogen-bond donor side of the chain becomes increasingly more positively charged, whereas the hydrogen-bond acceptor side of the chain becomes increasingly more negatively charged (see Figure 6 and Table 2). For example, the squaramide dimer has Voronoi deformation density (VDD) atomic charges of +205 and −205 milli-electrons at the first and last monomers, respectively. This charge separation increases to +227 and −233 milli-electrons at the first and last monomers of the squaramide tetramer, respectively. Therefore, the electrostatic attraction becomes more pronounced every time a new monomer is added to the chain not only from the attraction between non-neighboring monomers (that is, the long-range electrostatic interaction) but also from the more pronounced charge separation in the chains. In the next part, we address how the C–C bonds of deltamide and squaramide become more equal upon the formation of the hydrogen-bonded linear chains.

Origin of the ring equalization

We recall that the major structural reorganization of the three- and four-membered rings of deltamide and squaramide is observed in the single C–C bonds, especially the C–C bond formed between the carbon atoms of the two carbonyl groups in the squaramide (C1–C2 bond), that shortens upon forming linear chains by 0.06 Å (see Figure 2). The equalization of the three- and four-membered rings upon forming linear chains was explained in earlier work by the gain of aromaticity due to the increase in π-delocalization.[5] We find that the shortening of the single C1–C2 bond is mainly due to the elongation of the carbonyl C=O bonds that participate in hydrogen bonding. In this work, we further investigate the mechanism for the contraction of the C1–C2 bond in the squaramide to reveal that this effect is attributed to the relief of steric Pauli repulsion between the two carbonyl carbons when the C=O bond is elongated upon hydrogen bond formation.

Firstly, we confirm that the elongation of the C=O bonds is the driving force behind the structural reorganization of the four-membered ring of the squaramide monomers upon the formation of the linear chains. To this end, we have performed numerical experiments in which we take one squaramide monomer, in its planar equilibrium geometry, and consistently elongate in equidistant steps: i) the two N1–H1 and N2–H3 bonds; and ii) the two C=O bonds, whereas all other geometrical parameters are allowed to relax. The variation of all

Table 2. Energy decomposition analysis (in kcal mol^{-1}) of the interaction between the chain ($n-1$ monomers system) and an additional monomer added at the hydrogen-bond acceptor side of the chain, VDD charge Q on the monomer (in milli-electrons), and the orbital energies **ε** (in eV) for urea, deltamide, and squaramide.[a,b]

System	n	ΔE_{int}	ΔV_{elstat}	ΔE_{Pauli}	ΔE_{oi}	$\Delta E_{oi,\sigma}$	$\Delta E_{oi,\pi}$	ΔE_{disp}	Q_1^{VDD}	Q_n^{VDD}	$\varepsilon(\sigma_{HOMO-m})$	$\varepsilon(\sigma^*_{LUMO})$
Urea	2	−10.0	−16.6	16.8	−7.8	−7.0	−0.8	−2.5	+147	−147	−9.5	−1.0
	3	−13.2	−19.1	17.1	−8.8	−7.8	−1.0	−2.5	+154	−160	−8.5	−1.6
	4	−14.2	−19.9	17.2	−9.0	−8.0	−1.0	−2.5	+155	−162	−8.2	−1.8
Deltamide	2	−13.6	−18.4	16.0	−8.3	−7.3	−1.0	−2.9	+159	−159	−8.3	−1.4
	3	−17.2	−21.3	16.4	−9.4	−8.2	−1.2	−2.9	+165	−172	−7.2	−2.0
	4	−18.4	−22.2	16.5	−9.8	−8.5	−1.3	−3.0	+168	−174	−6.8	−2.3
Squaramide	2	−16.3	−27.2	29.8	−15.5	−13.6	−1.9	−3.4	+205	−205	−9.8	−1.7
	3	−22.0	−31.6	30.2	−17.1	−14.8	−2.3	−3.4	+221	−226	−8.7	−2.5
	4	−23.9	−33.2	30.3	−17.6	−15.3	−2.3	−3.4	+227	−233	−8.3	−2.8

[a] Computed at BLYP-D3(BJ)/TZ2P; Q_1^{VDD} is the VDD charge on the first monomer of the chain; Q_n^{VDD} is the VDD charge on the terminal monomer of the chain after formation of the hydrogen bonds; ε is the orbital energy of the associated fragment molecular orbital (FMO) in the $n-1$ monomer (σ_{HOMO-1} for urea; σ_{HOMO-1} for deltamide; σ_{HOMO-3} for squaramide). [b] Similar results are found when the chain elongates by adding a new monomer to the hydrogen-bond donor side of the chain (Table S5).

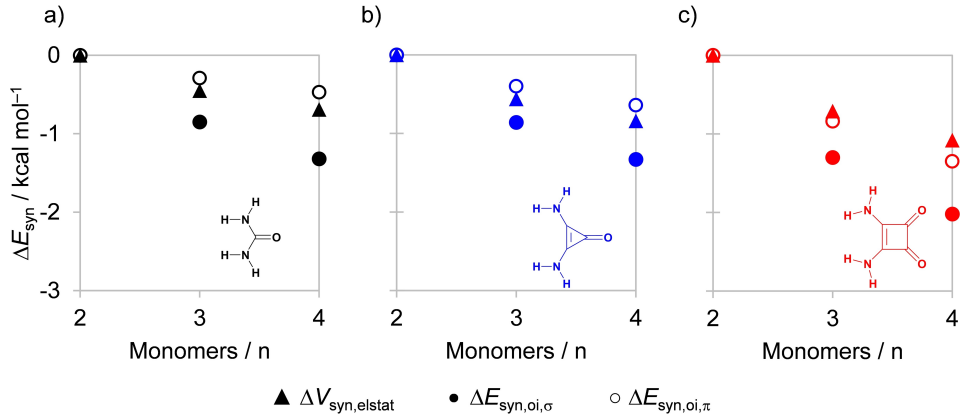

Figure 5. Energy decomposition diagrams of the average synergy for a) urea (black), b) deltamide (blue), and c) squaramide (red) linear chains with n monomers, computed at BLYP-D3(BJ)/TZ2P. For the full data set, see Table S4 in the Supporting Information.

C–C bond lengths as a response to the N–H or C=O bond lengthening is shown in Figure 7. The small contraction of the N–C bonds upon hydrogen bonding is not relevant as this slightly elongates the C1–C2 single bond (see Figure S3 in the Supporting Information). We find that all C–C bond lengths remain nearly unchanged when elongating the N1–H1 and N2–H3 bonds (see Figure 7a). The elongation of the C=O bond, on the other hand, causes immediate changes in the C–C bonds of the four-membered ring of the squaramide, predominantly in the C1–C2 bond that significantly shortens (see Figure 7b). The same outcome can be found when performing the same numerical experiment for the deltamide (see Figure S3) and the non-aromatic oxalaldehyde (see Figure 7c), *i.e.*, the C–C bond significantly shortens as both C=O bonds elongate. Therefore, we conclude that the changes in the C–C bond lengths in the squaramide ring are a secondary effect in response to the elongation of the C=O bonds caused by the hydrogen bond formation between the monomers in the linear chain.

To establish the causal relationship between the C=O bond elongation and the C1–C2 bond contraction in squaramide, we have performed a second numerical experiment in which we elongate the C=O bonds of the oxalaldehyde, while keeping all other atomic coordinates frozen, *i.e.*, all carbons and hydrogens remain in the same position in space. The oxalaldehyde acts as a simplified model to reproduce similar effects observed in the squaramide for two reasons: i) the oxalaldehyde is a smaller molecule that contains only the O=C–C=O fragment and two hydrogen atoms; and ii) experiences the same crucial geometrical deformations as the squaramide, that is, its C–C bond significantly shortens as both C=O bonds elongate. To this end, the oxalaldehyde starting geometry in this second experiment is taken from the coordinates of the O=C–C=O fragment of the squaramide in its planar equilibrium geometry. Thereafter, the hydrogen atoms have been added and only their coordinates have been optimized. Next, we analyze the bonding mechanism of the C–C bond formation from two HOC· open-shell fragments.

The activation strain and energy decomposition analyses of the C–C bond formation in our oxalaldehyde model are projected onto the C=O bond stretch, $\Delta r_{C=O}$, and shown in Figure 8. Herein, all energy terms are relative to the starting point $\Delta r_{C=O} = 0$, that is, the change in C=O bond length in the

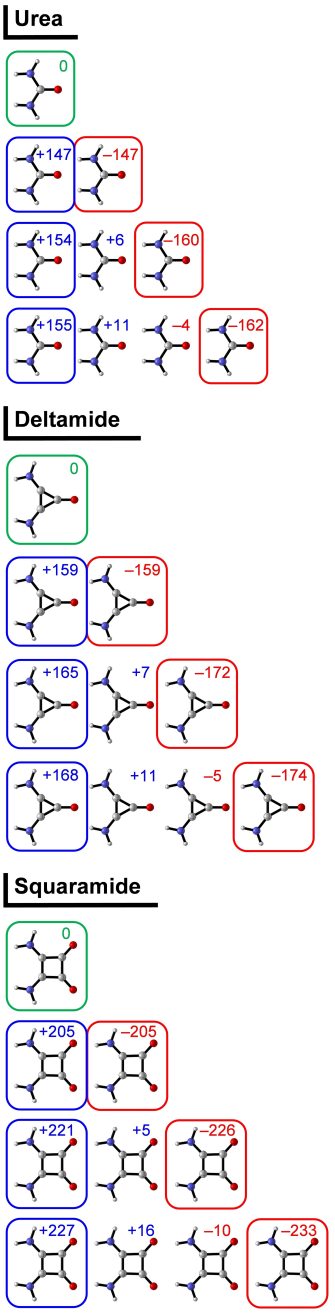

Figure 6. VDD charges Q (in milli-electrons) for the monomers of cooperative urea, deltamide, and squaramide systems, computed at BLYP-D3(BJ)/TZ2P. Blue corresponds to $Q > 0$, green to $Q = 0$, and red to $Q < 0$.

squaramide linear chain. We find that the total energy curve, $\Delta\Delta E$, is dictated by the strain energy curve, $\Delta\Delta E_{strain}$, which reflects the energy penalty of expanding the C=O bonds (see Figure 8a). The interaction energy curve, $\Delta\Delta E_{int}$, becomes increasingly more stabilizing as the C=O bonds elongate, but not enough to overcome the highly destabilizing $\Delta\Delta E_{strain}$. Thus, the expansion of the C=O bonds and, therefore, the contraction of the C–C bond does not occur without an energetic compensation. In the urea, deltamide, and squaramide linear chains, for example, this energetic cost for expanding the C=O bonds is compensated by the stabilizing hydrogen bonds between the monomers upon formation of the linear chain.

Next, we see that the interaction energy curve becomes increasingly more stabilizing mainly due to the reduction in steric Pauli repulsion, $\Delta\Delta E_{Pauli}$, which is the driving force for the C–C bond contraction in the oxalaldehyde model (Figure 8b). The π-electronic orbital interactions curve, $\Delta\Delta E_{oi,\pi}$, also favors the formation of the C–C bond but descends less steep than $\Delta\Delta E_{Pauli}$. The electrostatic interaction, $\Delta\Delta V_{elstat}$, is the only term that opposes the formation of the C–C bond, since it becomes less stabilizing when the two carbonyl oxygen atoms are further away, decreasing the attractive overlap of charge distributions.[14]

As the C=O bond expands, the electron density polarizes towards the most electronegative atom of the bond, *i.e.*, the oxygen atom. Consequently, the amplitude of the σ_{HOMO} C=O bonding orbital on the carbon atom of the HOC· fragment is decreased, causing the reduction of the repulsive $\langle\sigma_{HOMO}|\sigma_{HOMO}\rangle$ orbital overlap within the C–C bond and, thus, decreasing the steric Pauli repulsion (see Figure 9). Note that the molecular orbitals (MO) of oxalaldehyde, emerging from the interaction between the fragment molecular orbitals (FMO) of the two HOC· fragments, resemble the carbonyl oxygen lone pair orbitals of squaramide (see Figure 4 and Figure S2c). The π-electronic orbital interactions play a secondary role favoring the C–C bond shortening as the C=O bonds lengthen. When the C=O bonds elongate, the π_{HOMO} donor orbital of the HOC· fragment becomes increasingly more destabilized and the π^*_{LUMO} acceptor orbital of the HOC· fragment becomes increasingly stabilized, resulting in a smaller π_{HOMO}–π^*_{LUMO} energy gap and, thus, more stabilizing orbital interactions (see Figure 9). Nevertheless, note that this extra stabilization by orbital interactions within the π-system is a response to the C=O bond elongation and not due to the gain in aromaticity associated with the strengthening of the π-delocalization in resonance-assisted hydrogen bonds (RAHB) when the chain lengthens.[5,8] The Pauli repulsion within the σ-system behaves as a barrier for the C–C contraction, and the reduction of this barrier allows all C–C bonds in a ring to be equalized, making the four-membered ring more regular. This mechanism is valid for aromatic and non-aromatic molecules as demonstrated by earlier studies,[9,15] and can be easily extrapolated to deltamides and squaramides. Therefore, the delocalization of the π-electrons in the RAHB is not the reason for the enhancement of the hydrogen-bond strength in linear chains and, ultimately, plays a minor role in the equalization of the C–C bonds.

Conclusions

In this work, we demonstrate and explain the cooperativity and structural deformations in hydrogen-bonded urea, deltamide, and squaramide linear polymers. All systems show a cooperative effect stemming from donor–acceptor orbital interactions within the σ-system, and not within the π-system. The cooperativity arises from the flow of charge from the oxygen lone pair orbital on one monomer towards the σ* N–H

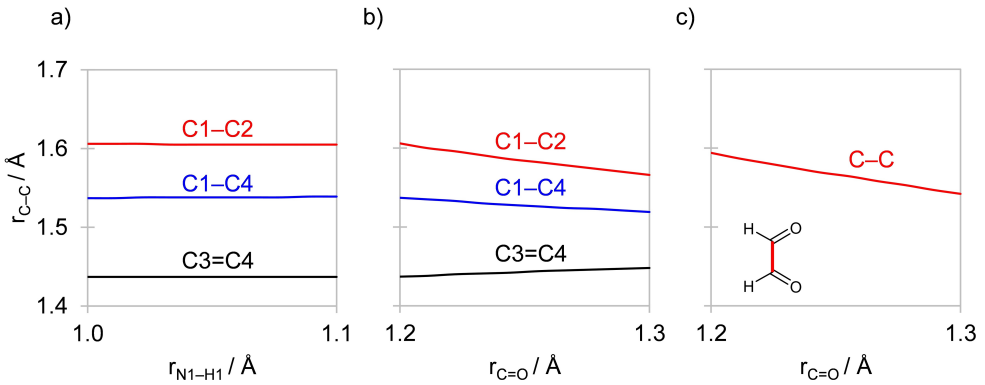

Figure 7. C–C bond lengths (in Å) projected onto the expansion of the a) N1–H1 and the symmetric equivalent N2–H3 bond for squaramide, b) C=O bonds for squaramide, and c) C=O bonds for the oxalaldehyde model. See Scheme 1 for the atom numbering. Note that C1–C4 is symmetric equivalent to C2–C3. Computed at BLYP-D3(BJ)/TZ2P.

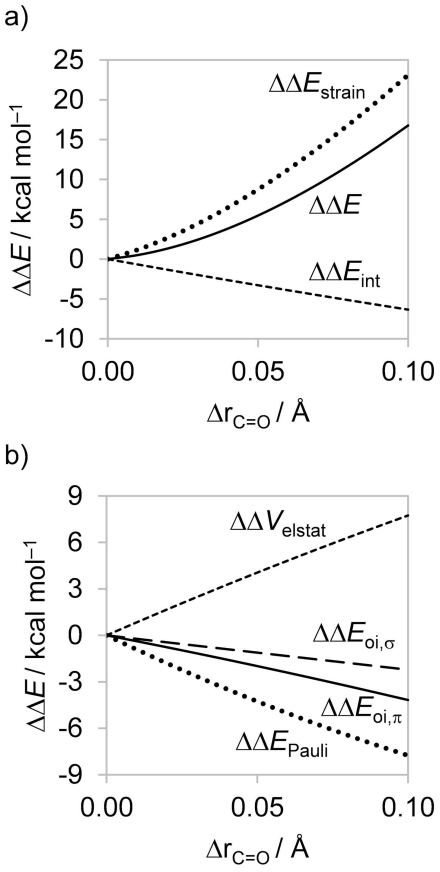

Figure 8. Variation of a) Activation strain and b) energy decomposition analysis energy terms along with the C=O bonds expansion (in Å) for the interaction between two HOC· open-shell model fragments. Computed at BLYP-D3(BJ)/TZ2P. For the full data set, see Tables S6 and S7 in the Supporting Information.

antibonding orbital on the interacting monomer that induces an increasingly pronounced charge separation along with the chain lengthening, resulting in a smaller donor–acceptor orbital energy gap. The π-electron delocalization does not significantly contribute to the increasingly strengthening of the studied hydrogen bonds upon polymerization. This follows from our dispersion-corrected density functional theory (DFT-D) calculations based on quantitative Kohn-Sham molecular orbital theory.

Our analyses reveal that the C–C bond length equalization in deltamide and squaramide linear chains is a direct consequence of the C=O bond elongation, induced by hydrogen bonding. For the squaramide, we find that the lengthening of the C=O ultimately causes the relief in Pauli repulsion between the occupied σ-type C=O bonding orbitals that have a lobe pointing towards the adjacent C–C bonds. This lobe, located on the carbon atoms, becomes consistently smaller as the more electronegative oxygen atoms are farther away, reducing the repulsive overlap within the C–C bond region and thereby shortening the C–C bond.

Lastly, we find that the π-electron delocalization within the monomers is also a response to the C=O bond expansion. The π C=O bonding donor orbital rises and the π C=O antibonding acceptor orbital drops in energy as the C=O bond becomes longer, leading to a smaller energy gap between occupied and unoccupied orbitals within the π-system and, therefore, more stabilizing orbital interactions. However, this gain in stabilization contributes much less to the ring motif equalization than the abovementioned relief in Pauli repulsion within the σ-electronic system between the carbonyl carbon atoms.

Theoretical Methods

Computational details

All calculations were carried out using the Amsterdam Density Functional (ADF) 2017.103 program.[16] All stationary points and energies were calculated at the BLYP level of the generalized gradient approximation (GGA); exchange functional developed by Becke (B), and the GGA correlation functional developed by Lee, Yang, and Parr (LYP)[17] (see Tables S8–S20 in the Supporting Information for the Cartesian coordinates). The DFT-D3(BJ) method developed by Grimme and coworkers,[18] which contains the damping function proposed by Becke and Johnson,[19] is used to describe non-local dispersion interactions. This level is referred to as BLYP-D3(BJ)/TZ2P and has been proven to accurately describe weak interactions.[3c] A large uncontracted relativistically optimized TZ2P

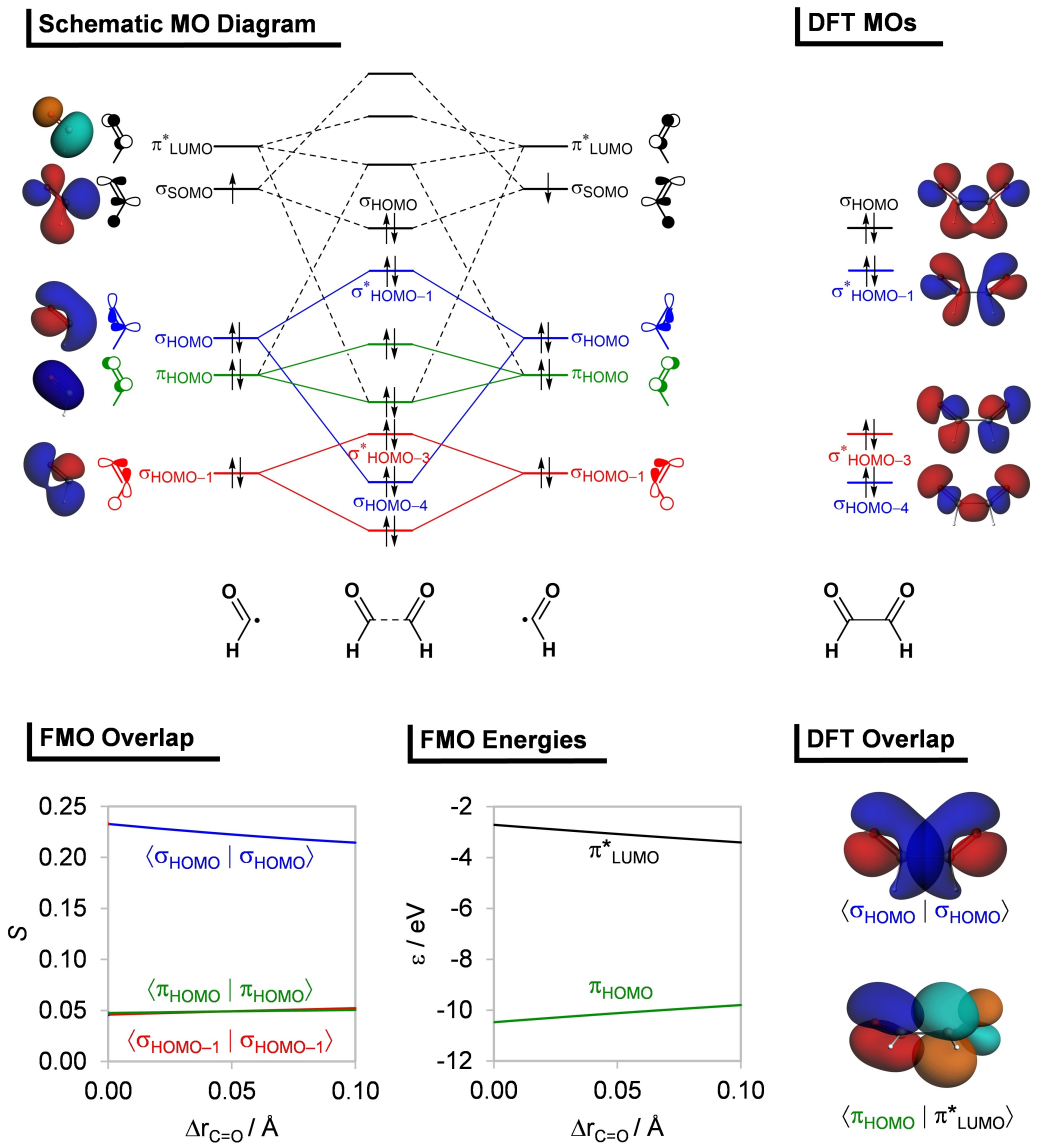

Figure 9. Molecular orbital (MO) diagram for the interaction between two HOC· open-shell model fragments, overlap between fragment molecular orbitals (FMO), and the resulting MOs of oxalaldehyde (isosurfaces at 0.04 a.u.). Computed at BLYP-D3(BJ)/TZ2P.

Slater type orbitals (STOs) basis set containing diffuse functions were used. The TZ2P all-electron basis set,[21] with no frozen-core approximation, is of triple-ζ quality for all atoms and has been augmented with the following sets of polarization and diffuse functions. Notably, previous studies on hydrogen-bonded systems have shown that the employed basis set, *i.e.*, TZ2P, gives a basis set superposition error (BSSE) of only a few tenths of a kcal mol^{-1} and hence this will not affect the computed trends in hydrogen bond strength.[12a,21] The molecular density is fitted by the systematically improvable Zlm fitting scheme.[22] Infinite chain geometries were computed using the BAND module at BLYP-D3(BJ)/TZ2P level under C_s symmetry, *i.e.*, planar chains (with the mirror plane in the plane of the molecule), and finite ground-state (closed-shell) fragments were cut out with a length of two till ten monomers.

Bond analysis

The bond energy ΔE of the chain with n monomers is defined as Eq. (1), where E_{chain} is the energy of the chain, $E_{monomer}$ is the energy of a single monomer in its equilibrium geometry, and n is the number of monomers in the chain.

$$\Delta E = E_{chain} - n \cdot E_{monomer} \quad (1)$$

According to the activation strain model (ASM),[23] ΔE comprises of two components, ΔE_{strain} and ΔE_{int}. In the framework of the Kohn-Sham molecular orbital model using quantitative canonical energy decomposition analysis (EDA),[10] the latter is further decomposed into electrostatic interaction, Pauli repulsion, orbital interaction to which a term ΔE_{disp} is added to account for the dispersion interaction [Eq. (2)].

$$\Delta E_{int} = \Delta V_{elstat} + \Delta E_{Pauli} + \Delta E_{oi} + \Delta E_{disp} \quad (2)$$

The usually attractive term ΔV_{elstat} corresponds to the classical Coulomb interaction between the unperturbed charge distributions of the deformed fragments. The Pauli repulsion ΔE_{Pauli} comprises

the destabilizing interactions between occupied orbitals of the fragments and is responsible for steric repulsion. The orbital-interaction energy ΔE_{oi} accounts for charge transfer, that is, the interaction between occupied orbitals of one fragment with unoccupied orbitals of the other fragment, including the interactions of the highest occupied and lowest unoccupied MOs (HOMO–LUMO), and polarization, that is, empty-occupied orbital mixing on one fragment, due to the presence of another fragment. The dispersion energy ΔE_{disp} accounts for the dispersion corrections as introduced by Grimme *et al.*[18] To facilitate the analyses, the ASM and EDA were performed using the PyFrag 2019 program.[24]

The orbital interaction energy can be further decomposed into the contributions from each irreducible representation of the interacting system [Eq. (3)].[25] In the systems considered in this study, it is possible to distinguish σ and π orbital interactions.

$$\Delta E_{oi} = \Delta E_{oi,\sigma} + \Delta E_{oi,\pi} \tag{3}$$

The average synergy, a measure to quantify the amount of cooperativity in the linear systems, is determined by comparing the average total interaction energy of the linear chain containing *n* monomers with the total interaction energy of a dimer [Eq. (4)].

$$\Delta E_{syn} = \left[\Delta E_{int}^{chain}/(n-1)\right] - \Delta E_{int}^{dimer} \tag{4}$$

Here, ΔE_{int}^{chain} is the total interaction energy of the linear chain with *n* monomers and ΔE_{int}^{dimer} is the total interaction energy of the dimer. A negative value of ΔE_{syn} corresponds to a positive cooperative effect in the chain, which reinforces the average total interaction energy. Equivalently, the average synergy of each EDA term is quantified according to the Eq. (5).

$$\Delta V_{syn,elstat} = \left[\Delta V_{elstat}^{chain}/(n-1)\right] - \Delta V_{elstat}^{dimer} \tag{5.1}$$

$$\Delta E_{syn,Pauli} = \left[\Delta E_{Pauli}^{chain}/(n-1)\right] - \Delta E_{Pauli}^{dimer} \tag{5.2}$$

$$\Delta E_{syn,oi} = \left[\Delta E_{oi}^{chain}/(n-1)\right] - \Delta E_{oi}^{dimer} \tag{5.3}$$

$$\Delta E_{syn,disp} = \left[\Delta E_{disp}^{chain}/(n-1)\right] - \Delta E_{disp}^{dimer} \tag{5.4}$$

The electron density distribution is analyzed using the Voronoi deformation density (VDD) method for computing atomic charges.[26] For better numerical sensitivity, the Voronoi grid has been used. The VDD atomic charge on atom X in a molecule (Q_X^{VDD}) is computed as the (numerical) integral of the deformation density in the volume of the Voronoi cell of X [Eq. (6)]. The Voronoi cell of X is defined as the compartment of space bounded by the bond midplanes on and perpendicular to all bond axes between nucleus X and its neighboring nuclei.

$$Q_X^{VDD} = -\int_{\text{Voronoi cell of X}} \left[\rho(r) - \rho_{promolecule}(r)\right] dr \tag{6}$$

Here, the deformation density is the difference between $\rho(r)$, *i.e.*, the electron density of the overall molecule or complex, and $\rho_{promolecule}(r) = \Sigma_Y \rho_Y(r)$, *i.e.*, the superposition of spherical average-of-configuration atomic densities $\rho_Y(r)$ of each atom Y in the fictitious promolecule without chemical interactions, in which all atoms are considered neutral. The interpretation of the VDD charge Q_X^{VDD} is rather straightforward and transparent: instead of measuring the amount of charge associated with X, Q_X^{VDD} directly monitors how much charge flows out of ($Q_X^{VDD} > 0$) or into ($Q_X^{VDD} < 0$) the Voronoi cell of X due to chemical interactions.

Acknowledgements

We thank the Netherlands Organization for Scientific Research (NWO) and the Dutch Astrochemistry Network (DAN) for financial support. This work was carried out on the Dutch national e-infrastructure with the support of SURF Cooperative.

Conflict of Interest

There are no conflicts to declare.

Keywords: cooperative effects · density functional calculations · energy decomposition analysis · hydrogen bonds · supramolecular chemistry

[1] a) G. R. Desiraju, *Angew. Chem. Int. Ed.* **1995**, *42*, 2311; b) R. Chakrabarty, P. S. Mukherjee, P. J. Stang, *Chem. Rev.* **2011**, *111*, 6810; c) S. I. Stupp, L. C. Palmer, *Chem. Mater.* **2014**, *26*, 507; d) B. Qin, Z. Yin, X. Tang, S. Zhang, Y. Wu, J.-F. Xu, X. Zhang, *Prog. Polym. Sci.* **2020**, *100*, 101167; e) H.-T. Feng, J. W. Y. Lam, B. Z. Tang, *Coord. Chem. Rev.* **2020**, *406*, 213142; f) A. Ciesielski, M. El Garah, S. Masiero, P. Samorì, *Small* **2016**, *12*, 83; g) J. Fan, X. Xu, W. Yu, Z. Wei, D. Zhang, *Polym. Chem.* **2020**, *11*, 1947; h) J. Li, L. Kan, J. Li, Y. Liu, M. Eddaoudi, *Angew. Chem. Int. Ed.* **2020**, *59*, 19659; *Angew. Chem.* **2020**, *132*, 19827; i) N. Kobko, L. Paraskevas, E. del Rio, J. J. Dannenberg, *J. Am. Chem. Soc.* **2001**, *123*, 4348.

[2] a) G. M. Whitesides, J. P. Mathias, C. T. Seto, *Science* **1991**, *254*, 1312; b) J. M. Lehn, *Science* **1993**, *260*, 1762.

[3] a) C. Fonseca Guerra, H. Zijlstra, G. Paragi, F. M. Bickelhaupt, *Chem. Eur. J.* **2011**, *17*, 12612; b) G. Paragi, C. Fonseca Guerra, *Chem. Eur. J.* **2017**, *23*, 3042; c) P. Vermeeren, L. P. Wolters, G. Paragi, C. Fonseca Guerra, *ChemPlusChem* **2021**, *86*. 812.

[4] a) S. Yamabe, K. Morokuma, *J. Am. Chem. Soc.* **1977**, *99*, 1316; b) A. E. Reed, F. Weinhold, L. A. Curtiss, D. J. Pochatko, *J. Chem. Phys.* **1986**, *84*, 5687; c) S. C. C. van der Lubbe, C. Fonseca Guerra, *Chem. Eur. J.* **2017**, *23*, 10249; d) S. C. C. van der Lubbe, C. Fonseca Guerra, *Chem. Asian J.* **2019**, *14*, 2760; e) C. Fonseca Guerra, F. M. Bickelhaupt, *Angew. Chem.* **1999**, *111*, 3120; *Angew. Chem. Int. Ed.* **1999**, *38*, 2942.

[5] a) G. Gilli, F. Bellucci, V. Ferretti, V. Bertolasi, *J. Am. Chem. Soc.* **1989**, *111*, 1023; b) H. R. Paudel, R. Das, C.-H. Wu, J. I. Wu, *Org. Biomol. Chem.* **2020**, *18*, 1078; c) Y. Chen, J. J. Dannenberg, *J. Am. Chem. Soc.* **2006**, *128*, 8100.

[6] a) L. Chen, S. N. Berry, X. Wu, E. N. W. Howe, P. A. Gale, *Chem* **2020**, *6*, 61; b) K. A. Agnew-Francis, C. M. Williams, *Chem. Rev.* **2020**, *120*, 11616; c) M. Zaleskaya, M. Karbarz, M. Wilczek, Ł. Dobrycki, J. Romański, *Inorg. Chem.* **2020**, *59*, 13749; d) A. P. Davis, S. M. Draper, G. Dunne, P. Ashton, *Chem. Commun.* **1999**, 2265; e) V. S. Talens, D. M. M. Makurat, T. Liu, W. Dai, C. Guibert, W. E. M. Noteborn, I. K. Voets, R. E. Kieltyka, *Polym. Chem.* **2019**, *10*, 3146.

[7] a) D. Quiñonero, R. Prohens, C. Garau, A. Frontera, P. Ballester, A. Costa, P. M. Deyà, *Chem. Phys. Lett.* **2002**, *351*, 115.

[8] a) V. S. Talens, P. Englebienne, T. T. Trinh, W. E. M. Noteborn, I. K. Voets, R. E. Kieltyka, *Angew. Chem. Int. Ed.* **2015**, *54*, 10502; *Angew. Chem.* **2015**, *127*, 10648; b) V. S. Talens, J. Davis, C.-H. Wu, Z. Wen, F. Lauria, K. B. S. S. Gupta, R. Rudge, M. Boraghi, A. Hagemeijer, T. T. Trinh, P. Englebienne, I. K. Voets, J. I. Wu, R. E. Kieltyka, *J. Am. Chem. Soc.* **2020**, *142*, 19907.

[9] a) S. Shaik, A. Shurki, D. Danovich, P. C. Hiberty, *Chem. Rev.* **2001**, *101*, 1501; b) S. C. A. H. Pierrefixe, F. M. Bickelhaupt, *Chem. Eur. J.* **2007**, *13*, 6321.

[10] a) F. M. Bickelhaupt, E. J. Baerends, in Reviews in Computational Chemistry, Vol. 15 (Eds.: K. B. Lipkowitz, D. B. Boyd), Wiley-VCH, New York, **2000**, pp. 1–86; b) T. A. Hamlin, P. Vermeeren, C. Fonseca Guerra, F. M. Bickelhaupt, in Complementary Bonding Analyses, (Ed.: S. Grabowski), De Gruyter, Berlin, **2021**, pp. 199–212.
[11] a) B. Behera, P. K. Das, *J. Phys. Chem. A* **2018**, *122*, 4481; b) A. Masunov, J. J. Dannenberg, *J. Phys. Chem. B* **2000**, *104*, 806; c) J. J. Dannenberg, L. Haskamp, A. Masunov, *J. Phys. Chem. A* **1999**, *103*, 7083.
[12] a) C. Fonseca Guerra, F. M. Bickelhaupt, J. G. Snijders, E. J. Baerends, *J. Am. Chem. Soc.* **2000**, *122*, 4117; b) L. P. Wolters, F. M. Bickelhaupt, *ChemistryOpen* **2012**, *1*, 96; c) A. A. Grosch, S. C. C. van der Lubbe, C. Fonseca Guerra, *J. Phys. Chem. A* **2018**, *122*, 1813.
[13] S. C. C. van der Lubbe, F. Zaccaria, X. Sun, C. Fonseca Guerra, *J. Am. Chem. Soc.* **2019**, *141*, 4878.
[14] a) D. Rodrigues Silva, L. de Azevedo Santos, T. A. Hamlin, F. M. Bickelhaupt, M. P. Freitas, C. Fonseca Guerra, *Phys. Chem. Chem. Phys.* **2021**, *23*, 20883; b) A. Krapp, F. M. Bickelhaupt, G. Frenking, *Chem. Eur. J.* **2006**, *12*, 9196.
[15] a) F. M. Bickelhaupt, E. J. Baerends, *Angew. Chem. Int. Ed.* **2003**, *42*, 4183; *Angew. Chem.* **2003**, *115*, 4315; b) D. Rodrigues Silva, L. de Azevedo Santos, T. A. Hamlin, C. Fonseca Guerra, M. P. Freitas, F. M. Bickelhaupt, *ChemPhysChem* **2021**, *22*, 641.
[16] ADF2017.103, SCM Theoretical Chemistry; Vrije Universiteit: Amsterdam, The Netherlands; http://www.scm.com.
[17] a) A. D. Becke, *Phys. Rev. A* **1988**, *38*, 3098; b) C. Lee, W. Yang, R. G. Parr, *Phys. Rev. B* **1988**, *37*, 785.
[18] a) S. Grimme, J. Antony, S. Ehrlich, H. Krieg, *J. Chem. Phys.* **2010**, *132*, 154104; b) S. Grimme, S. Ehrlich, L. Goerigk, *J. Comput. Chem.* **2011**, *32*, 1456.
[19] E. R. Johnson, A. D. Becke, *J. Chem. Phys.* **2005**, *123*, 024101.
[20] N. Mardirossian, M. Head-Gordon, *Mol. Phys.* **2017**, *115*, 2315.
[21] E. van Lenthe, E. J. Baerends, *J. Comput. Chem.* **2003**, *24*, 1142.
[22] M. Franchini, P. H. T. Philipsen, E. van Lenthe, L. Visscher, *J. Chem. Theory Comput.* **2014**, *10*, 1994.
[23] a) F. M. Bickelhaupt, *J. Comput. Chem.* **1999**, *20*, 114; b) W.-J. van Zeist, F. M. Bickelhaupt, *Org. Biomol. Chem.* **2010**, *8*, 3118; c) P. Vermeeren, T. A. Hamlin, F. M. Bickelhaupt, *Chem. Commun.* **2021**, *57*, 5880; d) P. Vermeeren, S. C. C. van der Lubbe, C. Fonseca Guerra, F. M. Bickelhaupt, T. A. Hamlin, *Nat. Protoc.* **2020**, *15*, 649.
[24] a) PyFrag 2007–2020: X. Sun, T. M. Soini, L. P. Wolters, W.-J. van Zeist, C. Fonseca Guerra, T. A. Hamlin, F. M. Bickelhaupt, Vrije Universiteit Amsterdam, The Netherlands; b) X. Sun, T. M. Soini, J. Poater, T. A. Hamlin, F. M. Bickelhaupt, *J. Comput. Chem.* **2019**, *40*, 2227.
[25] T. Ziegler, A. Rauk, *Inorg. Chem.* **1979**, *18*, 1558.
[26] a) F. M. Bickelhaupt, N. J. R. van Eikema Hommes, C. Fonseca Guerra, E. J. Baerends, *Organometallics* **1996**, *15*, 2923; b) C. Fonseca Guerra, J.-W. Handgraaf, E. J. Baerends, F. M. Bickelhaupt, *J. Comput. Chem.* **2004**, *25*, 189.

Manuscript received: September 29, 2021
Revised manuscript received: October 18, 2021
Accepted manuscript online: October 19, 2021